Cement and Concrete Research 42 (2012) 665–672

Contents lists available at SciVerse ScienceDirect

Cement and Concrete Research

journal homepage: http://ees.elsevier.com/CEMCON/default.asp

Hydration and percolation at the setting point

George W. Scherer [a,*], Jie Zhang [b], John A. Quintanilla [c], Salvatore Torquato [d]

[a] Princeton University, Dept. Civil & Env. Eng./PRISM, Eng. Quad. E-319, Princeton, NJ 08544 USA
[b] Princeton University, Dept. Civil & Env. Eng., Eng. Quad. E-228, Princeton, NJ 08544 USA
[c] University of North Texas, Dept. Mathematics, Denton, TX 76203-5017 USA
[d] Princeton University, Dept. Chemistry/PRISM/PCTS/PACM, Princeton, NJ 08544 USA

ARTICLE INFO

Article history:
Received 25 August 2011
Accepted 7 February 2012

Keywords:
Hydration (A)
Kinetics (A)
Elastic moduli (C)
Rheology (A)

ABSTRACT

The setting of cement paste is widely understood to be caused by percolation of the links that are created by overlap of hydration products on the surfaces of reacting grains of clinker. Percolation theory predicts that the elastic modulus will increase with a certain functional form, but few attempts have been made to demonstrate this behavior quantitatively. We discuss the appropriate variables to use for this test of the theory, and show that the percolation probability is proportional to time only over a narrow time interval. We compare the measured and predicted degree of hydration at the percolation threshold, and show that the hard-core/soft-shell model strongly over-estimates the amount of hydration at the setting point. The discrepancy is attributed to agglomeration of particles in the paste, which reduces the amount of hydration needed to link the particles into an elastic network.

© 2012 Elsevier Ltd. All rights reserved.

1. Introduction

The setting of cement paste is generally understood to be a percolation process in which the hydration products that form on the surface of clinker particles intersect, leading to the formation of clusters that eventually join into a continuous elastic network. The percolation of the solid and pore phases has been investigated using numerical simulations, the earliest of which was by Bentz and Garboczi, using CEMHYD [1]. That paper predicted a high degree of hydration at the percolation threshold, but later work produced lower, more realistic, values [2]; the difference apparently resulted from increasing the spatial resolution used in the simulation [3]. Similar studies have been done using HYMOSTRUC to predict the fraction of connected solids [4]. The connection between the percolation of solids and the rise in elastic modulus has also been examined by comparing various measures of rigidity, such as the Vicat test or sound velocity, with the degree of connectivity simulated with CEMHYD [5–7] or HYMOSTRUC [4,8]. Only a few studies have tried to quantify the change in properties near the setting point in terms of percolation theory, but each of those analyses has defects that will be discussed.

The purpose of this paper is to re-examine the use of percolation theory for interpreting the setting behavior of cement paste. The analysis will be demonstrated by using data for the ultrasonic pulse velocity and chemical shrinkage obtained in an earlier study [9]. We will then compare the observed threshold to the prediction of the hard-core/soft-shell (HCSS) percolation model developed by Torquato et al. [10, Ch. 10 of ref. 11], which is particularly relevant to setting of cement paste.

2. Percolation theory

2.1. Lattice and continuum percolation

In its simplest form, percolation theory describes the growth of clusters as particles are placed on the sites of a lattice, or as bonds are established between particles in an array. The probability of filling a site or forming a bond is p, and it is found that a continuous network (or, infinite cluster) is formed at a critical value, $p = p_C$, called the percolation threshold. In the vicinity of the threshold, many properties (P) of the network obey power-laws, such as

$$P \propto (p - p_C)^{\gamma} \tag{1}$$

where γ is called a critical exponent [12]. The value of p_C depends on the geometry of the lattice, but the critical exponents do not (for systems in which connections are made only between nearest neighbors [11]).

It has been demonstrated that the percolation threshold occurs at a fixed volume fraction of connected particles (or area fraction, in two-dimensional lattices) [12], which makes it practical to apply percolation theory to physical problems. This is called continuum percolation, because it assumes that the percolating objects are placed at random in continuous space, rather than on a lattice. The critical exponents for geometrical properties (such as the cluster size distribution) are identical for continuum and lattice percolation, but the exponents for transport properties may be different. For example, if

* Corresponding author. Tel.: 1 609 258 5680.
E-mail address: scherer@princeton.edu (G.W. Scherer).

0008-8846/$ – see front matter © 2012 Elsevier Ltd. All rights reserved.
doi:10.1016/j.cemconres.2012.02.003

equal-sized balls of glass and aluminum are randomly mixed, then the mixture will become electrically conducting when the volume fraction of aluminum particles, ϕ, exceeds $\phi_C \approx 16$ vol.%, which is the percolation threshold in 3-d [12]. In this case, the conductivity, σ, would vary as

$$\sigma \propto (\phi - \phi_C)^{\tau} \tag{2}$$

where the exponent $\tau \approx 1.6$–2 in 3-d (with more recent analyses favoring the higher value) (Ch. 9 of ref. 11[12]). In this example, the percolating objects are non-overlapping spheres, and they exhibit the same exponent as a lattice model. Feng et al. [13] showed that the conductivity exponent for overlapping spheres (what they call the "inverse Swiss-cheese model") is also the same as τ for a lattice model; however, if random spherical voids are placed in a conducting continuum, then the exponent rises by 0.5. The change in τ is attributed to the influence of very tenuous links that are created when two voids are close together; in contrast, all of the links in a lattice model have equal conductivity.

Models for the elastic behavior of percolating systems show a broad range of critical behavior. For a system described by an isotropic Born potential, in which relative displacements of particles in any direction generate the same force (a situation called *scalar*, or *isotropic*, *elasticity*), the shear modulus is expected to exhibit the same critical exponent as σ [14,15]; however, under purely central forces, a higher exponent (on the order of 3.4–4.4 [16]) and a higher percolation threshold are predicted to apply [14]. The Born potential is not rotationally invariant (i.e., it indicates that interparticle forces result from a rotation of the whole body), so it is not clear that it provides a correct representation for any physical system. Lattice models in which bonds resist both stretching and bending yield a critical exponent of $\gamma \approx 4$ for the elastic modulus [13], and continuum models with overlapping spheres are predicted to have $\gamma \approx 4.5$ in 3-dimensions.

Some experimental studies show the higher exponents, and some seem to indicate that there is a crossover from lower to higher values as the degree of connectivity increases [16]. On the other hand, studies of gelation of polymers usually indicate an exponent near 2 (e.g., [17]), as do studies of the setting of cement [18]. In general, the form of Eq. (1) applies only in the immediate vicinity of the percolation threshold, because it is only one term in a series expansion, and there is no way to anticipate its range of applicability a priori. It is possible that the theoretically predicted exponents only apply in a very narrow range of p–p_C that is not captured by the experiments. Well beyond the threshold, conventional composite models will apply, and these predict a nearly parabolic dependence on the volume fraction of solids [19,20]. A further complication is that hard spheres exhibit highly nonlinear elastic behavior, as they oppose being pushed together, but not being pulled apart [21]. In the case of an HCSS particle, the ratio of resistance to compression versus tension depends on the thickness of the shell and the magnitude of the strain.

The development of the modulus during setting of cement paste has been measured by rheometry e.g., [22] and acoustic methods [22–30]. In most cases, the increase in stiffness was correlated with the degree of connectivity calculated from a numerical simulation [4,5,8,27,31]. In one case [31], the calculated amount of connected solids was used together with an assumed critical exponent of $\gamma = 1.53$ to find the constant of proportionality in Eq. (2); however, the modulus data were compromised by entrapped air in the sample, as explained in the next section. Another study [8] used a similar procedure, but applied Eq. (2) to data very far from the percolation threshold (>36 h of hydration), where the theory is not expected to apply. Boumiz et al. [18] analyzed acoustic data in terms of percolation theory by assuming that the progress of the percolation process could be approximated by replacing p–p_C with the elapsed time, t–t_C. This is valid if the rate of the process is constant in time, but that is an assumption that needs to be verified. We will demonstrate in Section 3 that it only applies in a very small time interval near the percolation threshold.

2.2. HCSS percolation

The standard version of continuum percolation theory clearly does not describe the setting of cement, where the volume fraction of solids is initially well above 16%. The particles in cement are not located randomly in space: they are dispersed in a liquid and, in the absence of aggregation,[1] it would be possible to put more than 60 vol.% particles into a slurry without forming a network. In the paste, the network forms as a result of the growth of hydration products on the surfaces of the clinker particles, so the quantity p–p_C must be related to the degree of hydration. This process is described by the HCSS model [11], where the hard core represents the unhydrated clinker and the soft shell represents the layer of hydration products. The shells overlap to link the particles into increasingly large clusters, leading to percolation. Although the geometry of this model is different from conventional continuum percolation, the same critical exponents apply [32]. The comparison of the HCSS model with data for Class H cement will be shown in Section 4.

3. Acoustic transmission

3.1. Slurries and networks

The velocity, V, of a longitudinal wave in a suspension is given approximately by [33]

$$K_M = \rho_M V^2 \tag{3}$$

where ρ_M and K_M are the mean density and bulk modulus of the suspension, which are defined by

$$\rho_M = \phi\rho_S + (1-\phi)\rho_F \tag{4}$$

and

$$\frac{1}{K_M} = \frac{\phi}{K_S} + \frac{1-\phi}{K_F} \tag{5}$$

where ρ_S and ρ_F are the densities, and K_S and K_F are the bulk moduli, of the suspended particles and the fluid medium, respectively; the mean density of a cement paste with w/c = 0.35 is $\rho_M \approx 2023$ kg/m^3. A more rigorous expression, which takes account of the frequency of the sound and the size of the suspended particles, was derived by Harker and Temple [33], and is discussed in Appendix 1. The effect of air on the velocity is shown in Fig. 1, where V drops below the speed of sound in air (~300 m/s) when the volume fraction of air exceeds ~0.1%; very similar results are obtained using Eq. (3). The impact of entrapped air was emphasized by Keating et al. [22], and the effect is clearly illustrated in Fig. 5 of Sant et al. [30]. In contrast, cement particles suspended in water are predicted to have a minor effect on V, as shown in Fig. 2. The particles cause some attenuation of the wave, but the effect is very small compared to that of air, as shown in Fig. 3.

[1] Throughout this paper, we use the term "aggregation" and "aggregate" to describe loose clusters of cement particles in the paste that have flocculated as a result of attractive van der Waals forces. These aggregates are to be distinguished from the rigid links created by overlapping hydration products, which lead to formation of an elastic network at the percolation threshold.

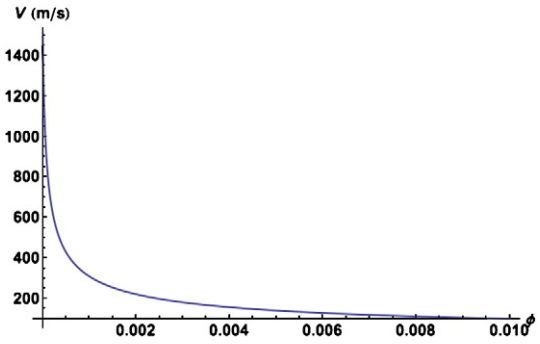

Fig. 1. Velocity of a longitudinal sound wave in water as a function of the volume fraction of air, ϕ, calculated using Eq. (14) with the property values given in Appendix 1.

When the particles are connected into a network, the propagation of sound is described by the theory developed by Biot [34,35]. When a cement paste sets, Sayers and Grenfell [36] argue that Biot's low-frequency limit applies:

$$\rho_M V^2 = M \tag{6}$$

where

$$M = K + \frac{4}{3}G + \frac{K_F(K_S - K)^2}{K_F(K_S - K) + K_S(K_S - K_F)(1-\phi)} \tag{7}$$

In Eq. (7), G and K are the drained shear and bulk moduli of the solid network, and ϕ is the volume fraction occupied by the network (which increases as hydration proceeds). In the limit when the network is extremely tenuous (K and $G << K_F$ or K_S), Eq. (7) reduces to

$$M \approx \frac{1}{\phi/K_S + (1-\phi)/K_F} = K_M \tag{8}$$

Thus, Eq. (6) becomes identical to Eq. (3) near the percolation threshold. To identify the point at which the network begins to form, we need to subtract those two equations. If we define the velocity in the suspension before percolation as $V_0 = \sqrt{K_M/\rho_M}$, then

$$\rho_M\left(V^2 - V_0^2\right) = K + \frac{4}{3}G \equiv H \tag{8}$$

where we introduce the longitudinal modulus of the network, H (also known as the oedometric modulus [37] or the stiffness c_{11} [38]).

The theory indicates that we should expect a longitudinal wave in a cement slurry to behave as shown in Fig. 4, beginning at about 1500 m/s and rising to a value typical of hardened cement as setting occurs; the increase begins at the percolation threshold when G and K take on finite values. The acoustic velocity data in Fig. 4 were

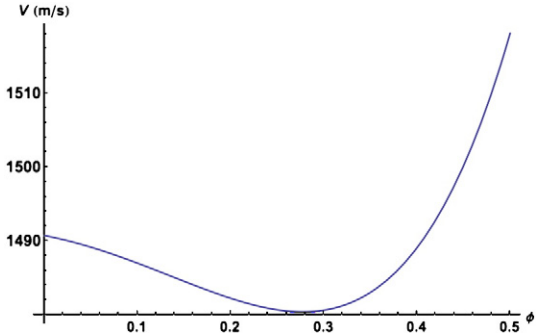

Fig. 2. Velocity of a longitudinal sound wave in water as a function of the volume fraction of cement particles in suspension, ϕ, calculated using Eq. (14) with the property values given in Appendix 1.

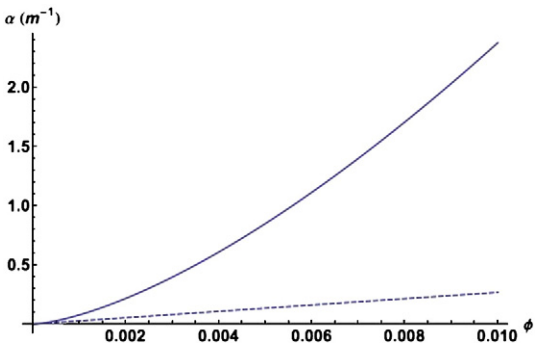

Fig. 3. Attenuation of a longitudinal wave as a function of the volume fraction, ϕ of air (solid curve) or cement particles (dashed curve), calculated using Eq. (15) with the property values given in Appendix 1.

obtained as part of a study reported earlier [9], where the procedure is described in detail. The plot shows the results of three runs, indicating that the reproducibility is excellent, so we will test the fit of percolation theory to these data.

It has been shown that colloids exhibit a rigidity threshold when the period of the acoustic wave is short compared to the lifetime of transient percolating clusters that form and disintegrate under the influence of Brownian agitation [39]. Clinker particles are too large to undergo Brownian diffusion [45], so the lifetime of aggregates is quite long compared to the period of the ultrasonic waves used in our experiments, but there is not enough mobility to cause transient percolation. The presence of agglomeration may contribute to the initial velocity measured in the slurry, but the rise in stiffness near the setting point is caused by the formation of elastic networks, which are also detected by low-frequency rheological measurements.

3.2. Percolation analysis of acoustic data

It is the modulus of the network that forms after percolation that is described by the power law, so we use Eqs. (1) and (8) to write

$$H = \rho_M\left(V^2 - V_0^2\right) \propto (p - p_C)^\gamma \tag{9}$$

Sayers and Grenfell [36] found that the moduli were proportional to each other after the percolation threshold, so G, K, and H must scale with the same exponent. We want to determine the critical exponent, γ, and percolation threshold, p_C. In the study by Boumiz et al. [18], they assumed that the rate of hydration was proportional to time, so that $p - p_C$ could be replaced by the elapsed time after the threshold,

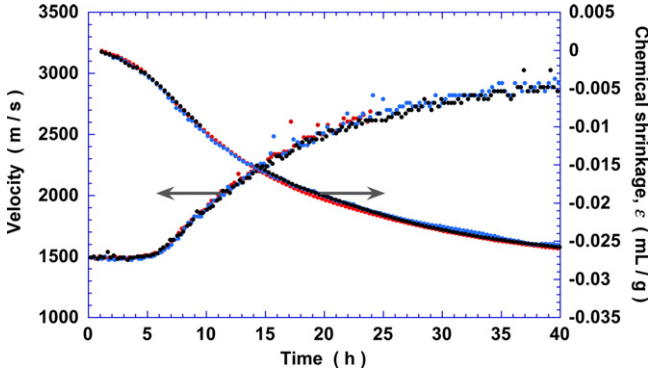

Fig. 4. Left ordinate: Measured velocity of longitudinal wave in Class H cement with water/cement ratio = 0.35, measured at 25 °C, as a function of time since contact with water; three runs over 2 weeks. Right ordinate: Chemical shrinkage of the same type of paste; three runs over 4 months.
Data from ref. [9].

t–t_C. We can test this assumption by making use of the shrinkage data that were collected for identical pastes, by the technique described in Ref. [9]. The chemical shrinkage strain, ε, is shown in Fig. 4. One might argue that chemical shrinkage is an indirect measure of the extent of reaction, but the shrinkage is linearly proportional to the degree of hydration, h, as shown in Fig. 5; the slope is $s=\varepsilon/h=-0.0764$ mL/(g clinker). The advantage of using ε is that it is recorded continuously with high resolution in time, as is the pulse velocity.

The velocity data were fit to the power law, using the absolute value of the chemical shrinkage to represent the parameter p, with c, $|\varepsilon_C|$, and γ as free parameters:

$$V^2-V_0^2=c(|\varepsilon|-|\varepsilon_C|)^{\gamma} \tag{10}$$

The fit, shown in Fig. 6, is very good; the power-law region extends up to about 20 h of hydration time, which is much later than the final setting time (~7–8 h) found from the Vicat needle test. The exponent is $\gamma=1.59$, which is lower than the value expected for scalar elasticity. Over this time interval, the longitudinal modulus has risen to about 10 GPa; after 90 h, the velocity reaches ~3100 m/s (not shown), which corresponds to $H\approx 19.4$ GPa. Thus, the power-law applies while the modulus rises to about half of its final value.

The velocity data are also fit quite well by an equation of the form

$$V^2-V_0^2=c(t-t_C)^{\gamma} \tag{11}$$

but only over a range from about 4 to 9 h. After that, the curvature reverses (becoming concave down toward the time axis). In that small interval, a good fit is obtained with $\gamma\approx 2.0$ (not shown), as was found by Boumiz et al. [18]. If the fit to Eq. (10) is limited to that time interval, the exponent is also found to be about 2, indicating that ε is linearly proportional to time over that period; however, the range of data is rather small for fixing 3 parameters. Nevertheless, since the exponent found for the wider range of time is lower than predicted by any percolation model, it is reasonable to conclude that a power-law fit to the smaller interval is most appropriate, in which case we can use either variable to represent p–p_C, and the critical exponent is very nearly $\gamma\approx 2$.

From the fit to Eq. (10), the chemical shrinkage at the percolation threshold is found to be $|\varepsilon_C|=0.00198$ mL/g, which occurs at about 3.9 h of hydration; the fit to Eq. (11) yields $t_C\approx 4.1$ h. Both times are significantly shorter than the time of initial set found by the Vicat

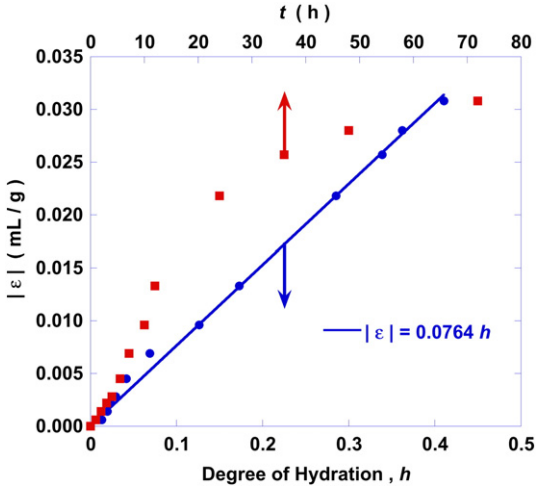

Fig. 5. Absolute value of the chemical shrinkage of Class H cement paste, $|\varepsilon|$, versus degree of hydration (lower abscissa) and time (upper abscissa). A linear fit of $|\varepsilon|$ as a function of h yields a slope of 0.0764 mL/g; the dependence of $|\varepsilon|$ on time is highly nonlinear over the same interval.
Data from ref. [9].

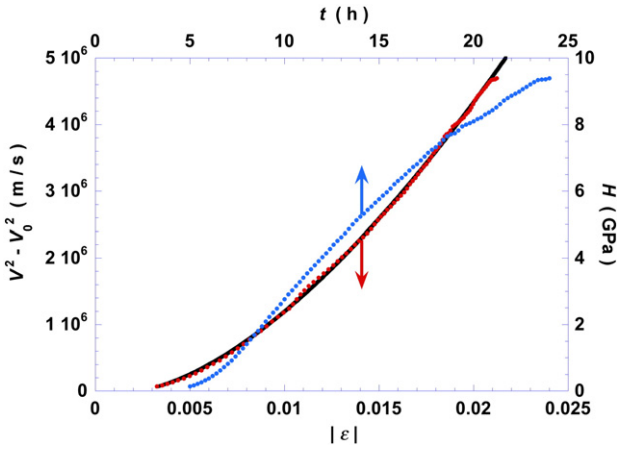

Fig. 6. Longitudinal velocity (symbols) plotted versus the absolute value of the chemical shrinkage, $|\varepsilon|$ (lower abscissa), and versus the time of hydration, t (upper abscissa). Solid curve is a fit to Eq. (10), which yields a critical exponent of $\gamma=1.59$; data from Fig. 4. Right ordinate is longitudinal modulus, calculated from acoustic velocity using Eq. (8) with $\rho_M=2023$ kg/m^3.

test, which was 5.5 h for this paste [9]. This disparity, which has also been observed in comparisons of the Vicat setting point with oscillatory rheology [40], occurs because the modulus at the percolation threshold is very much smaller than the yield stress (around 40 kPa [41]) detected by the Vicat needle.

If no data on chemical shrinkage or degree of hydration are available, a reasonably accurate estimate of the time of percolation can be obtained using time as a variable, as suggested by Boumiz et al. [18]. One can assume that $\gamma=2$ in Eq. (11), and fit the following equation to the data:

$$\sqrt{V^2-V_0^2}=c'(t-t_C) \tag{12}$$

This is only valid if there is no entrapped air, so that V_0 is ~1500 m/s, and it can only be expected to work in a small time interval around t_C, where the plot is linear. An example of such a fit is shown in Fig. 7 for the same data as in Fig. 6.

When comparing the acoustic and shrinkage measurements, it is important to recognize that the paste in the shrinkage experiment is covered with water, and the sample is relatively small, so there is not likely to be any self-desiccation during the test. In contrast, the acoustic sample is covered with oil, so it is possible that hydration would be more limited than for the shrinkage sample after setting occurs. In the present case, this is unlikely, because the Class H cement is relatively coarse, and shows severe bleeding at w/c as low

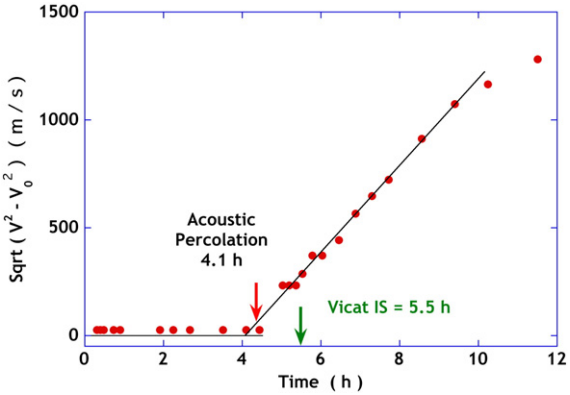

Fig. 7. Approximate percolation fit to acoustic data using Eq. (12); velocity data are the same as in Fig. 6.

as 0.4, which is why our tests were run at w/c = 0.35. However, for ordinary cement pastes, the degree of hydration at low w/c might be different in shrinkage and acoustic experiments after setting occurs. The difference could be mitigated by putting a layer of water over the acoustic sample, and covering that with oil to suppress evaporation, or by covering the shrinkage sample with oil, instead of water.

The present data, as well as the results of simulations and experiments reported in the literature, are consistent with the idea that setting of cement paste results from percolation of the particles. This means that setting is a geometrical phenomenon: for a given initial volume fraction of clinker, setting will occur at a fixed degree of hydration, independent of temperature, pressure, or the use of accelerators or retarders (as long as those factors do not change the nature of the hydration product). These expectations are borne out experimentally [9,42]. We should, therefore, be able to use percolation theory to predict the degree of hydration at which setting of a paste will begin for a given water/cement ratio and particle size distribution. We will attempt to do this by application of the HCSS model.

4. Percolation and setting

If equally sized non-overlapping spheres are placed at random in a box, they will percolate at a volume fraction of about 16%, so another approach is needed to reach the high solids loadings of cement paste. The HCSS simulation begins by arranging particles in a box on a lattice, and then shifting their positions with a Metropolis algorithm to achieve a random distribution. If one were to try to shift the particles so as to minimize their energy of interaction, crystallization would occur for any solids loading exceeding ~49 vol.% [43,44]. This does not happen in a real cement paste, because the particles are polydisperse, and they are too large to undergo Brownian diffusion [45]. In the simulation, however, the rearrangement must be stopped at some stage prior to crystallization, when the particles are in a metastable arrangement in which they are as widely separated as possible. This is an important feature of this model, because the initial arrangement is well dispersed, whereas cement paste shows some degree of agglomeration [46], even when dispersants are used [47]. The consequences of this will become apparent.

Once the hard cores of the particles are in place, each can be expanded by an amount that corresponds to the thickness of the soft shell. The ratio of the diameter of the core, D_C, to that of the shell of the particle, D_P, is the "impenetrability parameter", $\lambda = D_C/D_P$. The volume fraction at which the shells percolate, ϕ_C, is shown as a function of λ in Fig. 8. We need to relate λ to the degree of hydration, h, of the clinker, so that we can use this theory to predict the percolation threshold for cement. The details of the calculation are explained in Appendix 2.

Based on the analysis in Appendix 2, we can relate the impenetrability parameter, λ, to the degree of hydration (DOH) of a hypothetical cement with uniform particle size. In Fig. 9, the predictions of the HCSS model are compared to values measured in Ref. [9]. The predicted DOH is much greater than the measured value, and the discrepancy increases with the water/cement ratio. The measured values correspond to the initial set found by the Vicat needle test, which occurs well after percolation, so the predicted DOH values should fall below the measurements. One might argue that the problem with the model is that it applies to monodisperse particles, whereas the particle size distribution in the actual cement ranges from about 0.5 to 90 μm [48]. To investigate the significance of this factor, four series of simulations were done in which several particle sizes from the measured distribution were included, with the ratio of the largest to smallest being 3:1 (with 10 sizes ranging from 0.239 to 0.717 μm), 6.25:1 (with 15 sizes, up to 1.49 μm), 10.2:1 (20 sizes, up to 2.43 μm), and 18.7:1 (25 sizes, up to 4.47 μm). The absolute sizes are small, but that does not matter, because only the relative sizes affect the percolation threshold. The particles, which represent the hard cores, were placed into the box, then a layer of uniform thickness was placed around each particle; that is, the depth of hydration was the same on particles of all sizes. For these simulations, a low density of particle cores was used, so the Metropolis algorithm was not applied; that is, the distribution achieved by random sequential addition of particles is statistically equivalent to the equilibrium distribution when the packing density is low. The layer thickness was increased until percolation occurred, with the results shown in Fig. 10; the calculated points are averages from at least 100, and usually ~1000 initial configurations. A short extrapolation of the simulated values is necessary to overlap with the w/c range of the data, but the values fall on very straight lines, so this is not expected to introduce a significant error. Again, the predictions are higher than the measured values, and the error increases with w/c; moreover, the discrepancy *increases* with the breadth of the particle size distribution in the simulation. This is probably a reflection of the fact that the smallest particles can hydrate completely without coming into contact with their neighbors, so they contribute to the DOH, but not to the formation of a network. We conclude that the failure of the model to capture the measured behavior is not related to the assumed particle size distribution.

The most likely cause of the discrepancy is the high degree of dispersion produced at the start of the simulation. This means that a high DOH is needed to produce a reaction layer thick enough to bring the

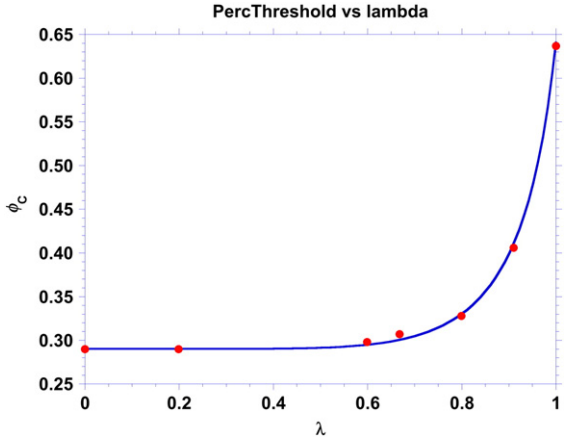

Fig. 8. Volume fraction of monodisperse hard-core/soft-shell particles (accounting for overlap of the shells) at the percolation threshold, as a function of the impenetrability parameter, λ. Curve is an empirical fit given in Eq. (22).
Data from Fig. 10.8 of ref. [11].

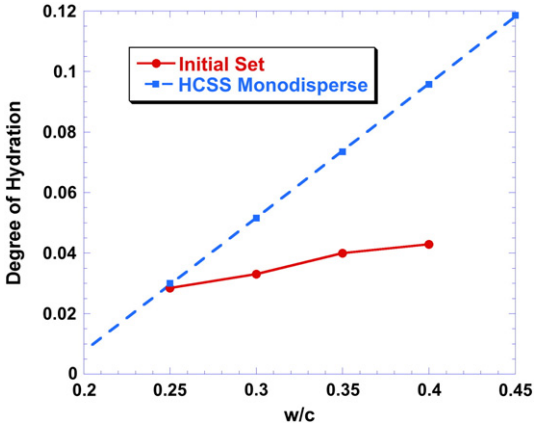

Fig. 9. Measured degree of hydration at the initial setting point found from the Vicat needle test (Initial Set) and calculated degree of hydration at the percolation threshold for equal-sized spheres (HCSS Monodisperse).
Data from ref. [9].

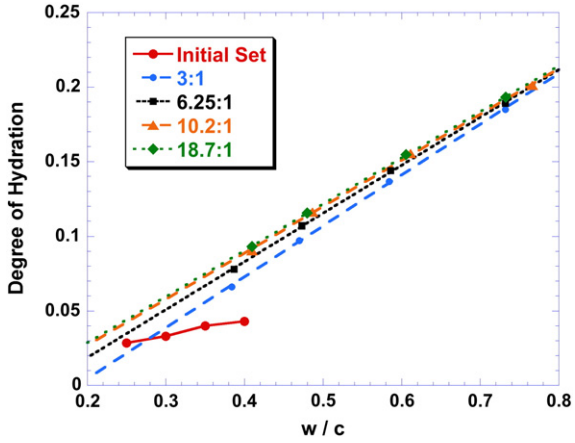

Fig. 10. Measured degree of hydration at the initial setting point found from the Vicat needle test (Initial set) and calculated degree of hydration at the percolation threshold for the HCSS model with polydisperse spheres with the indicated range of sizes. Data from ref. [9].

particles into contact. In contrast, real cement pastes contain large clusters of particles that are initially touching [46,47], so they can be bonded by the formation of a small amount of hydration product. This idea has been tested in a study in which the initial extent of agglomeration of the particles was systematically varied [49]; as expected, realistic predictions of DOH can be obtained with reasonable degrees of agglomeration. Several other simulation studies have predicted rather low DOH at the percolation threshold (e.g., [2,27]), but they did not optimize the particle spacing at the start of the process. Evidently, the methods used for random placement of particles into the box in those studies resulted in many of the particles being in very close proximity. Unfortunately, it is difficult to quantify the initial state of agglomeration of a paste, and without that information one cannot predict the DOH at the percolation threshold.

The critical exponent for the elastic modulus of a percolating HCSS system is expected to be much higher than what we observe [11,13]. The physical origin of the high exponent is the very broad range of stiffness of the linkages created by overlapping particles: deep interpenetration of particles creates very stiff links, while tangency creates flexible ones. The thinner the soft shell, the smaller the range of variation in stiffness will be, since overlapping is limited to the depth of the shell. Moreover, the aggregation of particles that occurs in a paste enhances the number of strong links, since the hydration products are depositing on particles already in contact, and that must alter the distribution of stiffnesses anticipated by the theory. These factors contribute to a reduction in the critical exponent from the high value ($\gamma \approx 4.1$–4.5) predicted for freely overlapping spheres. Since the initial setting of cement occurs at a low DOH (~4% for w/c = 0.35 [9]), the shell of hydration products is very thin at the setting point, so the elasticity of the cement system should approach the behavior of a hard-sphere model, and become subject to the nonlinearity mentioned earlier [21]. To our knowledge, the critical exponent for such a system has not been established theoretically.

5. Conclusions

When measurements of the acoustic velocity in hydrating cement paste are analyzed in terms of percolation theory, the expected power law behavior is observed for the elastic modulus, but the observed exponent is difficult to rationalize. If the degree of reaction is assumed to be linearly proportional to time, the fit is good over a narrow window in time (~4 to 9 h), and it yields a critical exponent of ~2.0. However, if the degree of reaction is represented by the chemical shrinkage, then the power-law applies over a much broader range of time (up to ~20 h), and the exponent is ~1.6. The latter is lower than the value predicted for systems exhibiting scalar elasticity, so fitting over the smaller time interval is more appropriate. A critical exponent of 2 is consistent with scalar elasticity, and is similar to values reported for gelation of polymers, but is much lower than the prediction for overlapping spheres. We conclude that setting is a percolation process, although the details of the process (viz., the evolution of the elastic properties) are not correctly captured by existing hard-core/soft-shell percolation models. The percolation threshold is reached well before the initial setting point defined by the Vicat needle test.

It would be convenient to have an analytical model to predict the degree of hydration at the setting point on the basis of the water/cement ratio and particle size distribution, so we tested the hard-core/soft-shell model. The model predictions were much higher than the measured DOH values, evidently because the simulations assume perfect dispersion of the particles, whereas actual pastes contain clusters of particles whose proximity allows them to become bonded by very thin reaction layers. Unfortunately, this means that the initial state of agglomeration must be known in order to predict the DOH at the percolation threshold.

Acknowledgments

The authors are indebted to Dale Bentz (NIST) for helpful discussions. S.T. was supported by the U.S. Department of Energy, Office of Basic Energy Sciences, Division of Materials Sciences and Engineering under Award DE-FG02-04-ER46108.

Appendix 1. Sound velocity in a suspension

Harker and Temple [33] derived the following expression (their equation 2.25) to describe the propagation of a longitudinal sound wave in a suspension:

$$\frac{\beta^2}{\omega^2} = \frac{\rho_F}{K_M}\left(\frac{\rho_S(1-\phi+\phi S)+\rho_F S(1-\phi)}{\rho_S(1-\phi)^2+\rho_F(S+\phi(1-\phi))}\right) \tag{13}$$

where β is the wave vector, ω is the radial frequency, K_M is defined in Eq. (5), and S is a complex quantity given by

$$S = \frac{1}{2}\left(\frac{1+2\phi}{1-\phi}\right)+\frac{9}{4}\left(\frac{\delta}{a}\right)+i\left(\frac{9}{4}\right)\left(\frac{\delta}{a}+\frac{\delta^2}{a^2}\right) \tag{14}$$

where a is the radius of the suspended particle and δ is the "skin depth" defined by

$$\delta = \sqrt{\frac{2\eta_F}{\omega\rho_F}} \tag{14}$$

and η_F is the viscosity of the fluid. The velocity of the longitudinal wave, V, is related to the real part of the wave vector,

$$V = \mathrm{Re}\left(\frac{\omega}{\beta}\right) \tag{14}$$

and the attenuation of the wave, α, is equal to its imaginary part:

$$\alpha = \mathrm{Im}(\beta) \tag{15}$$

The values in Fig. 1–Fig. 3 were calculated using the following values: $\omega = 2\pi\times10^5$ Hz; (for water) $\eta_F = 0.001$ Pa·s, $\rho_F = 1000$ kg/m^3, $K_F = 2.2$ GPa; (for clinker) $\rho_S = 3100$ kg/m^3, $K_S = 117$ GPa [50], $a = 10$ μm; (for air) $\rho_S = 1.2$ kg/m^3, $K_S = 10^5$ Pa, $a = 1$ μm.

Appendix 2. HCSS model

The parameters of the HCSS model described in Ref. [11] (hereafter, RHM) can be related to the properties of a partially hydrated cement particle as follows. If the initial diameter of the clinker particle is D_0 and the diameter of the unhydrated core is D_C, then the degree of hydration is

$$h = 1-\left(\frac{D_C}{D_0}\right)^3 \tag{16}$$

If the densities of the clinker and the hydration products are ρ_C and ρ_H, respectively, then the volumetric expansion, e, upon hydration is $e=\rho_C/\rho_H$; given $\rho_C\approx 3150\ \mathrm{kg/m^3}$ and $\rho_H\approx 2000\ \mathrm{kg/m^3}$, we have $e\approx 1.58$. The volume of the partially hydrated particle, with diameter D_P, is

$$v_P = \left(\frac{\pi}{6}\right)D_P^3 = \left(\frac{\pi}{6}\right)\left[D_C^3 + e\left(D_0^3-D_C^3\right)\right] = \left(\frac{\pi}{6}\right)D_0^3(1-h+he) \tag{17}$$

The RHM parameter ρ is the number density of particle cores and $N=\rho\, L^3$ is the number of particles in the system. The initial volume fraction of clinker particles is

$$\phi_0 = \frac{N(\pi/6)D_0^3}{L_0^3} = \left(\frac{\pi}{6}\right)D_0^3\rho_0 = \frac{1}{1+R_{wc}\rho_C/\rho_W} \tag{17}$$

The final equality in Eq. (17) relates the volume fraction to the water/cement ratio, R_{wc}; ρ_W is the density of water ($=1000\ \mathrm{kg/m^3}$). The subscripts on L_0 and ρ_0 are needed, because the volume of the system contracts during hydration, owing to chemical shrinkage. The change in volume of the system per particle is

$$\Delta V_H = \varepsilon\rho_C\left(\frac{\pi}{6}\right)D_0^3 = sh\rho_C\left(\frac{\pi}{6}\right)D_0^3 \tag{17}$$

where ε is the chemical shrinkage (in mL/g of clinker) and s (<0) is the ratio of ε to the degree of hydration, h (i.e., the negative of the slope of Fig. 5). The volume of the box at any stage of hydration is

$$L^3 = N\left(\frac{\pi}{6}\right)D_0^3(1+sh\rho_C) \tag{18}$$

so

$$\rho = \frac{\rho_0}{1+sh\rho_C} \tag{19}$$

From Fig. 5, $s=-0.0764$ mL/g, so when hydration is complete ($h=1$), Eq. (19) indicates that $\rho/\rho\approx 1.317$.

The RHM parameter η represents the extended volume fraction of solid phase (cores plus hydrated layer, ignoring overlap of the shells):

$$\eta = \rho v_P = \phi_0\left(\frac{1-h+he}{1+sh\rho_C}\right) = \frac{1-h+he}{(1+R_{wc}\rho_C/\rho_W)(1+sh\rho_C)} \tag{20}$$

The RHM parameter λ is the ratio of the diameter of the hard core, D_C, to that of the whole particle, D_P:

$$\lambda = \frac{D_C}{D_P} = \left(\frac{1-h}{1-h+he}\right) \tag{20}$$

According to eq. (5.119) on p. 155 of RHM, the volume fraction of solid phase (cores plus hydrate, taking account of overlap) is

$$\phi = 1-\left(1-\eta\lambda^3\right)\exp\left[-\frac{\left(1-\lambda^3\right)\eta}{\left(1-\eta\lambda^3\right)^3}\right]A(\eta,\lambda) \tag{21}$$

where

$$A(\eta,\lambda) = \exp\left[\begin{array}{l} -\dfrac{\eta^2\lambda^3(\lambda-1)}{2\left(1-\eta\lambda^3\right)^3} \\ \times\left(\left(7\lambda^2+7\lambda-2\right)-2\eta\lambda^3\left(7\lambda^2-5\lambda+1\right)+\eta^2\lambda^6\left(5\lambda^2-7\lambda+2\right)\right)\end{array}\right] \tag{22}$$

The value of the volume fraction at which percolation of the soft shells occurs, ϕ_C, is shown in Fig. 8. The curve is an empirical fit to the points, which is given by

$$\phi_C\approx 0.29+\frac{0.35\lambda^7}{2-\lambda^7} \tag{22}$$

The degree of hydration at the percolation threshold, h_C, is found by setting Eq. (21) equal to Eq. (22), and solving numerically for h for given values of R_{wc}, s, and e. This was done using *Mathematica*® [51].

References

[1] D.P. Bentz, E.J. Garboczi, Percolation of phases in a three-dimensional cement paste microstructural model, Cement Concr. Res. 21 (1991) 325–344.
[2] D.P. Bentz, P.V. Coveney, E.J. Garboczi, M.F. Kleyn, P.E. Stutzman, Cellular automaton simulations of cement hydration and microstructure development, Modelling Simul Mater. Sd. Eng. 2 (1994) 783–808.
[3] E.J. Garboczi, D.P. Bentz, The effect of statistical fluctuation, finite size error, and digital resolution on the phase percolation and transport properties of the NIST cement hydration model, Cement Concr. Res. 31 (2001) 1501–1514.
[4] G. Ye, K. van Breugel, A.L.A. Fraaij, Three-dimensional microstructure analysis of numerically simulated cementitious materials, Cement Concr. Res. 33 (2003) 215–222.
[5] A. Princigallo, P. Lura, K. van Breugel, G. Levita, Early development of properties in a cement paste: a numerical and experimental study, Cement Concr. Res. 33 (2003) 1013–1020.
[6] J.W. Bullard, M. D'Ambrosia, Z. Grasley, W. Hansen, N. Kidner, D. Lange, P. Lura, T.O. Mason, J. Moon, F. Rajabipour, G. Sant, S. Shah, Z. Sun, T. Voigt, S. Wansom, J. Weiss, L. Woo, in: J. Marchand, B. Bissonnette, R. Gagne, M. Jolin, F. Paradis (Eds.), 2nd Int. RILEM Symp. Advances in Concrete through Science and Engineering, September 2006, p. 307, Quebec, Canada.
[7] D.P. Bentz, A review of early-age properties of cement-based materials, Cement Concr. Res. 38 (2008) 196–204.
[8] Z. Sun, G. Ye, S.P. Shah, Microstructure and early-age properties of Portland cement paste—effects of connectivity of solid phases, ACI Mater. J. (2005) 122–129 ([March-April] Title no. 102-M15).
[9] J. Zhang, E.A. Weissinger, S. Peethamparan, G.W. Scherer, Early hydration and setting of oil well cement, Cement Concr. Res. 40 (2010) 1023–1033.
[10] S.B. Lee, S. Torquato, Pair connectedness and mean cluster size for continuum-percolation models: computer-simulation results, J. Chem. Phys. 89 (10) (1988) 6427–6433.
[11] S. Torquato, Random Heterogeneous Media, Springer, New York, 2002.
[12] R. Zallen, The Physics of Amorphous Solids, Wiley, New York, 1983 (Ch. 4).
[13] S. Feng, B.I. Halperin, P.N. Sen, Transport properties of continuum systems near the percolation threshold, Phys. Rev. B 35 (1) (1987) 197–214.
[14] S. Feng, P.N. Sen, Percolation on elastic networks: new exponent and threshold, Phys. Rev. Lett. 52 (3) (1984) 216–219.
[15] P.G. de Gennes, On a relation between percolation theory and the elasticity of gels, J. Phys. (Letters) 37 (1976) L1–L2 [Jan.].
[16] C.J. Brinker, G.W. Scherer, Sol–Gel Science, Academic Press, New York, 1990 (Ch. 5).
[17] T. Fujii, T. Yano, H. Kumagai, O. Miyawaki, Scaling analysis on elasticity of agarose gel near the sol–gel transition temperature, Food Hydrocolloids 14 (2000) 359–363.
[18] A. Boumiz, C. Vernet, F. Cohen Tenoudji, Mechanical properties of cement pastes and mortars at early ages, Adv. Cement-Based Mater. 3 (1996) 94–106.
[19] R.K. Bordia, G.W. Scherer, On constrained sintering: II. Comparison of constitutive models, Acta Metall. 36 (9) (1988) 2399–2409.
[20] L.J. Gibson, M.F. Ashby, Cellular Solids, Structure & Properties, Pergamon Press, New York, 1988.
[21] S. Torquato, A. Donev, F.H. Stillinger, Breakdown of elasticity theory for jammed hard-particle packings: conical nonlinear constitutive theory, Int. J. Solids Struct. 40 (2003) 7143–7153.
[22] J. Keating, D.J. Hannant, A.P. Hibbert, Comparison of shear modulus and pulse velocity techniques to measure the build-up of structure in fresh cement pastes used in oil well cementing, Cement Concr. Res. 19 (1989) 554–566.
[23] J. Keating, D.J. Hannant, A.P. Hibbert, Correlation between cube strength, ultrasonic pulse velocity and volume change for oil well cement slurries, Cement Concr. Res. 19 (1989) 715–726.

[24] R. D'Angelo, T.J. Plona, L.M. Schwartz, P. Coveney, Ultrasonic measurements on hydrating cement slurries onset of shear wave propagation, Advn. Cem. Based Mater. 2 (1995) 8–14.
[25] A. Feylessoufi, F. Cohen Tenoudji, V. Morin, P. Richard, Early ages shrinkage mechanisms of ultra-high-performance cement-based materials, Cem. Concr. Res. 31 (2001) 1573–1579.
[26] G. Ye, K. van Breugel, A.L.A. Fraaij, Experimental study and numerical simulation on the formation of microstructure in cementitious materials at early age, Cem. Concr. Res. 33 (2003) 233–239.
[27] G. Ye, P. Lura, K. van Breugel, A.L.A. Fraaij, Study on the development of the microstructure in cement-based materials by means of numerical simulation and ultrasonic pulse velocity measurement, Cem. Concr. Compos. 26 (2004) 491–497.
[28] N. De Belie, C.U. Grosse, J. Kurz, H.-W. Reinhardt, Ultrasound monitoring of the influence of different accelerating admixtures and cement types for shotcrete on setting and hardening behaviour, Cem. Concr. Res. 35 (2005) 2087–2094.
[29] G. Trtnik, G. Turk, F. Kavčič, V.B. Bosiljkov, Possibilities of using the ultrasonic wave transmission method to estimate initial setting time of cement paste, Cement Concr. Res. 38 (11) (2008) 1336–1342.
[30] G. Sant, M. Dehadrai, D. Bentz, P. Lura, C.F. Ferraris, J.W. Bullard, J. Weiss, Detecting the fluid-to-solid transition in cement pastes, Concrete international, June 2009, pp. 53–58, (+21 pages of supplementary information).
[31] G. Ye, Z. Sun, T. Voigt, K. van Breugel, S.P. Shah, A micromechanic model for characterization of cement paste at early age validated with experiments, Proc. RILEM Int. Symp. Advances in Concrete through Science and Engineering, Evanston, Ill, 2004, (CD-ROM) 11 pp.
[32] S.B. Lee, S. Torquato, Monte Carlo study of correlated continuum percolation: universality and percolation thresholds, Physical Review A 41 (10) (1990) 5338–5344.
[33] A.H. Harker, J.A.G. Temple, Velocity and attenuation of ultrasound in suspensions of particles in fluids, J. Phys. D: Appl. Phys. 21 (1988) 1576–1588.
[34] M.A. Biot, Theory of propagation of elastic waves in a fluid-saturated porous solid. I. Low-frequency range, J. Acoustical Soc. of Am. 28 (2) (1956) 168–178.
[35] M.A. Biot, Theory of propagation of elastic waves in a fluid-saturated porous solid. II. Higher frequency range, J. Acoustical Soc. of Am. 28 (2) (1956) 179–191.
[36] C.M. Sayers, R.L. Grenfell, Ultrasonic propagation through hydrating cements, Ultrasonics 31 (3) (1993) 147–153.
[37] O. Coussy, Poromechanics, Wiley, West Sussex, England, 2004.
[38] J.F. Nye, Physical Properties of Crystals: Their Representation by Tensors and Matrices, Clarendon Press, Oxford, 1985.
[39] L. Ye, J. Liu, P. Sheng, J.S. Huang, D.A. Weitz, Sound propagation in colloidal systems, J. de Physique IV, Colloque C1, supplement au J. Physique II 3 (1993) 183–196 [Mai].
[40] G. Sant, C.F. Ferraris, J. Weiss, Rheological properties of cement pastes: a discussion of structure formation and mechanical property development, Cem. Concr. Res. 38 (2008) 1286–1296.
[41] D. Lootens, P. Jousset, L. Martinie, N. Roussel, R.J. Flatt, Yield stress during setting of cement pastes from penetration tests, Cem. Concr. Res. 39 (5) (2009) 401–408.
[42] G.W. Scherer, G.P. Funkhouser, S. Peethamparan, Effect of pressure on early hydration of class H and white cement, Cement Concr. Res. 40 (2010) 845–850.
[43] M.D. Rintoul, S. Torquato, Metastability and crystallization in hard-sphere systems, Phys. Rev. Lett. 77 (1996) 4198–4201.
[44] M. Hermes, E.C.M. Vermolen, M.E. Leunissen, D.L.J. Vossen, P.D.J. van Oostrum, M. Dijkstra, A. van Blaaderen, Nucleation of colloidal crystals on configurable seed structures, Soft Matter 7 (2011) 4623–4628.
[45] N. Roussel, A. Lemaître, R.J. Flatt, P. Coussot, Steady state flow of cement suspensions: a micromechanical state of the art, Cem. Concr. Res. 40 (2010) 77–84.
[46] A. Chougnet, T. Palermo, A. Audibert, M. Moan, Rheological behaviour of cement and silica suspensions: particle aggregation modelling, Cem. Concr. Res. 38 (2008) 1297–1301.
[47] E. Sakai, T. Kasuga, T. Sugiyama, K. Asaga, M. Daimon, Influence of superplasticizers on the hydration of cement and the pore structure of hardened cement, Cem. Concr. Res. 36 (2006) 2049–2053.
[48] S. Peethamparan, E. Weissinger, J. Vocaturo, J. Zhang, G.W. Scherer, Monitoring chemical shrinkage using pressure sensors, ACI Special Proceedings in CD on Advances in the Material Science of Concrete, SP-270, 2010, pp. 77–88.
[49] J. Zheng, J. Zhang, G.W. Scherer, Prediction of the degree of hydration at initial setting time of cement paste with particle agglomeration, Cem. Concr. Res. (submitted for publication).
[50] G. Constantinides, F.-J. Ulm, The effect of two types of C-S-H on the elasticity of cement-based materials: results from nanoindentation and micromechanical modeling, Cem. Concr. Res. 34 (2004) 67–80.
[51] Inc Wolfram Research, Mathematica, Version 8.0, , 2010 (Champaign, IL).